OUTWARDLY PROPAGATING FLAMES AT ELEVATED PRESSURES

C. K. Law,[1] G. Rozenchan,[1] S. D. Tse[2] and D. L. Zhu[1]

[1]Department of Mechanical and Aerospace Engineering
Princeton University, Princeton, NJ 08544

[2]Department of Mechanical and Aerospace Engineering
Rutgers, The State University of New Jersey, Piscataway, NJ 08854

ABSTRACT

Spherical, outwardly-propagating flames of CH_4-O_2-inert and H_2-O_2-inert mixtures were experimentally studied in a high pressure apparatus. Stretch-free flame speeds and Markstein lengths were extracted for a wide range of pressures and equivalence ratios for spherically-symmetric, smooth flamefronts and compared to numerical computations with detailed chemistry and transport, as well as existing data in the literature.

Wrinkle development was examined for propagating flames that were unstable under our experimental conditions. Hydrodynamic cells developed for most H_2-air and CH_4-air flames at elevated pressures, while thermal-diffusive instabilities were also observed for lean and near-stoichiometric hydrogen flames at pressures above atmospheric. Strategies in suppressing or delaying the onset of cell formation have been assessed. Buoyancy effects affected sufficiently off-stoichiometric CH_4 mixtures at high pressures.

INTRODUCTION

For the present work, we adopted a recently-developed novel experimental apparatus for the investigation of elevated pressure H_2 and CH_4 flames [1-3], capable of conducting experiments up to 60 atm, and that allows for the direct imaging of a near-constant-pressure outwardly propagating flame. Using this apparatus, the laminar burning rates and downstream Markstein lengths of H_2-O_2-inert and CH_4-O_2-inert mixtures were experimentally and computationally obtained. The laminar flame speed, s_u^0, is a fundamental thermochemical parameter of the flame, embodying information about the diffusive and reactive aspects of a combustible mixture, and has been extensively used to validate detailed reaction mechanisms. The Markstein length, which characterizes and quantifies the flame response to stretch, is an indicator of the effective Lewis number of the combustible mixture, as it embodies the accelerating/decelerating tendency of the flame as it propagates, subject to positive/negative stretch, as well as the nonequidiffusive nature of the flame. The occurrence (or absence) of thermal-diffusional instabilities over the flame gives this reasoning further support.

EXPERIMENTAL AND COMPUTATIONAL METHODS

Apparatus and Instrumentation - The experimental apparatus consists of two coaxial cylindrical chambers. The inner chamber has quartz discs on both ends for optical access, and is initially filled with the combustible mixture. The outer chamber has quartz windows mounted in the end caps, and is initially filled with an inert mixture. There are matching rows of holes on the lateral

wall of the inner chamber and on its encasing sleeve which allow for continuity between the two chambers, when aligned; once offset, these holes are isolated via O-rings.

The reactants were mixed by a jet-stirring apparatus. The mixtures were ignited by a spark discharge and the flame propagation was optically recorded using Schlieren cinematography and a high-speed camera. Both chambers are equipped with digital pressure gages, used for filling the mixtures. Operational details, error analysis and system specifications can be found in Refs. 1-4.

Filling and Ignition Procedures - The individual components were introduced to the inner chamber according to the partial pressure method. Mixing and rest periods took place for ~10 minutes each. Homogeneity of the mixture could be visually inspected through the Schlieren system. The encasing sleeve was then translated, establishing continuity between the chambers, and the quiescent mixture was simultaneously ignited. Flame propagation was terminated when the flame reached the walls of the inner chamber, with the total pressure buildup attenuated due to the volume ratio between the two chambers. Therefore, a near-constant-pressure flame was established.

The temperature of the initial combustible mixture was kept at 298 ± 3K, and the ignition energy was adjusted to be close to its minimum value to achieve ignition, reducing its influence of initial flame acceleration.

Data Reduction - Measurements were restricted to spherical, smooth flames having diameters between 10 and 40 mm to avoid spark and wall effects. Results were averaged over 3-4 measurements for each point. Linear extrapolation [5,6] was chosen to obtain the unstretched flame speed (s_b^0) and the Markstein length (L_b), according to the relation $s_b = R = s_b^0 - L_b\kappa$, where κ is the stretch rate given by $\kappa = 2\dot{R}/R$. Substituting κ in the expression for $\dot{R}$ and integrating, we get the final correlation [7]: $R + 2L_b \ln R = s_b^0 t + C$, where, by measuring the flame radius (R) versus time, one can obtain L_b and s_b^0 by linear regression, after filtering the data for high-frequency noise. The unburned flame speed (s_u^0) is obtained by dividing s_b^0 by the density ratio of the planar flame through continuity.

From the concept of a one-step overall reaction, overall reaction orders (n) were extracted from both the experimental and computational data on the s_u^0 vs. pressure plots, according to the relation $n = 2 + 2[\partial \ln s_u^0 / \partial \ln p]$ that comes from dimensional analysis [8,9].

Numerical computations - The experimentally determined laminar flame speeds were compared to those of planar, adiabatic, one-dimensional premixed flames calculated by the Sandia PREMIX code [10]. H_2 flames were simulated using a detailed reaction mechanism including 9 species and 21 elementary reactions [11], CH_4/air flames with 53 species and 325 reactions (GRI-Mech 3.0) [12], and CH_4/O_2/He flames with 35 species and 217 reactions (GRI-Mech 3.0 without N-containing species and reactions). Third-body efficiency factors for Ar were used for He, and Soret effects were included. Adaptive gridding was used to map the flame structure. Radiative heat loss was not included. The unburned mixture temperature at the cold boundary was set at 298K, and zero gradients were imposed at the burned boundary.

RESULTS AND DISCUSSION

Experimental data on H_2-air and CH_4-air mixtures at 1 atm as a function of equivalence ratio has been compared with results from existing literature, and the good agreement provides a benchmark of accuracy for the present setup. These comparisons, along with plots of H_2 and CH_4 flame speeds as a function of equivalence ratio for different pressures can be found in Refs. 2-4. Figure 1 presents laminar flame speeds, Markstein lengths and overall reaction orders as a function of pressure for different H_2-O_2-inert mixtures. Discrepancies between experiments and com-

putations can be attributed to little validation of the mechanism used for the rich branch, uncertainties on H-atom diffusion properties and on the third body efficiency of He.

Figure 2 shows laminar flame speeds and Markstein lengths as a function of pressure for different CH_4-O_2-He mixtures. In general, for both H_2 and CH_4 mixtures, laminar flame speeds and Markstein lengths decrease with pressure, while L_b increases with equivalence ratio for a given pressure. The decrease in L_b with pressure is due to the decrease in flame thickness, while the decrease in s_u^0 follows from the fact that $n < 2$ for most of the mixtures studied (see exception for low pressures in Figs. 1a and 1c), meaning that the overall density increase outweighs the increase in concentration in the Arrhenius rate expression. Third-body termination reactions, such as $H+O_2+M \leftrightarrow HO_2+M$ are also favored at high pressures, contributing to this outcome by lowering n. Overall reaction orders decrease with pressure for H_2-air, H_2-O_2-He and CH_4-air mixtures, and increase with pressure for CH_4-O_2-He mixtures.

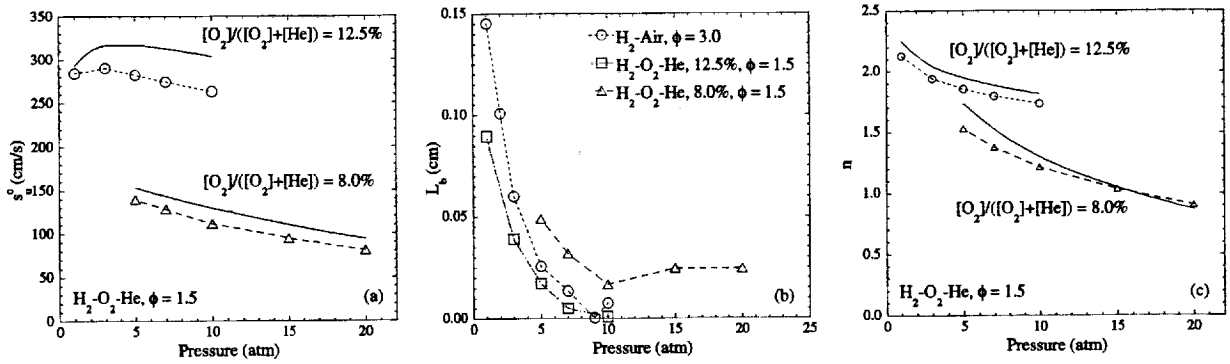

Fig. 1. Variation of flame properties of H_2-O_2-inert mixtures at fixed equivalence ratios with pressure: (a) laminar flame speed, (b) Markstein length and (c) overall reaction order. Symbols represent experimental data; lines represent simulation.

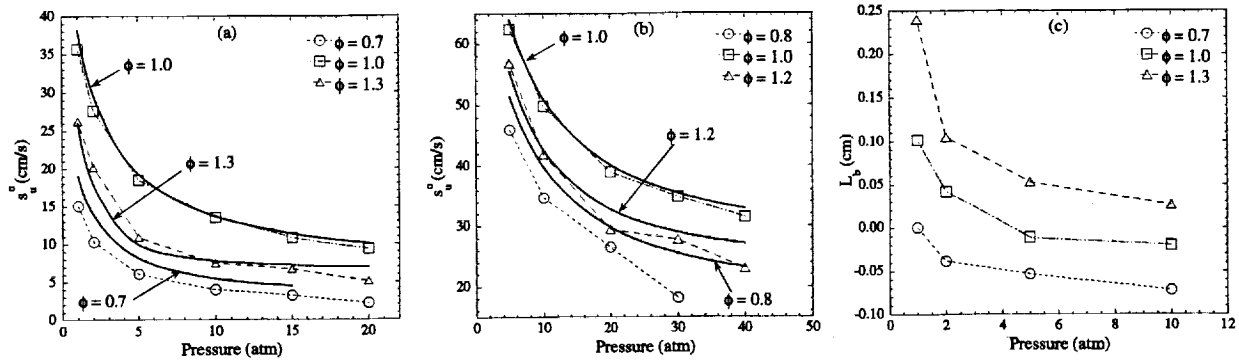

Fig. 2. Variation of laminar flame speed of (a) CH_4-air and (b) CH_4-O_2-He, $O_2/(He+O_2)$ = 17% mixtures at fixed equivalence ratios with pressure; (c) variation Markstein length of CH_4-air mixtures with pressure. Symbols represent experimental data; lines represent simulation.

Smooth flame speeds could only be measured for H_2-air flames at 1 atm (for all ϕ) or at very high ϕ (for higher pressures). At 2 atm, most lean and near-stoichiometric H_2-air flames are already unstable to hydrodynamic and thermal-diffusive instabilities, as seen in Fig. 3. Flames 3a and 3b have the same adiabatic flame temperature, but the former has $L_b > 0$ (and hence Le > 1, which makes it stable to thermal-diffusive cells [9]), while the latter has $L_b < 0$ (Le < 1). Fig. 3a also shows that large wrinkles, characterizing hydrodynamic cells, are formed first, while the thermal-diffusive cells (of smaller size and evenly distributed throughout the flame surface) have their onset at a later stage of propagation. CH_4-air flames do not manifest any thermal-diffusive

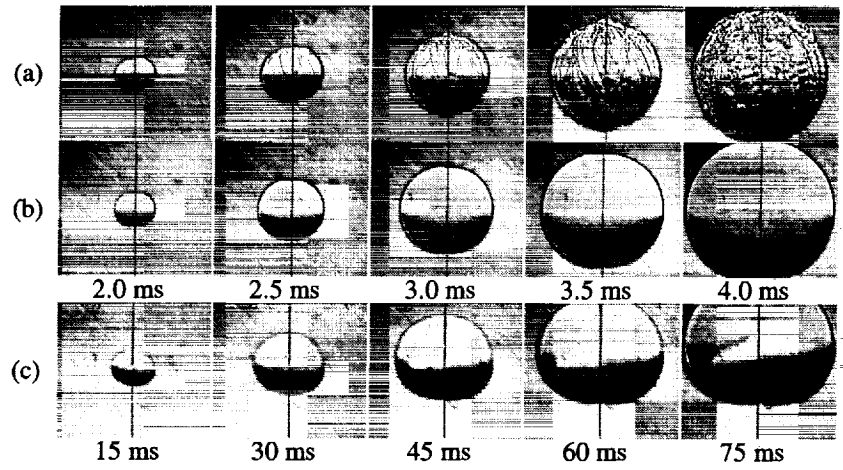

Fig. 3. Schlieren pictures of H_2-air flames at 2 atm: (a) $\phi = 0.56$, (b) $\phi = 3.00$. In (c) CH_4-air, 2 atm, $\phi = 0.60$.

cells up to 40 atm (even for negative L_b), being unstable only to hydrodynamic wrinkles above 10 atm. Part of this phenomenon might be due to the stabilizing effect of positive stretch in the outwardly-propagating flame [13], and part due to the size of the chamber used. Thermal-diffusive instabilities have been reported for CH_4-air flames at such pressures [14], but their onset is delayed until a critical radius is reached. Two strategies were devised to delay the onset of instabilities: higher O_2 dilution with inert in the oxidizer, weakening the flame and therefore reducing the effect of thermal expansion; and replacement of N_2 with He as inert, thereby increasing the mixture's Le. Both strategies also increase the flame thickness, hence damping the baroclinic torque across the flame that supports hydrodynamic instabilities. They have extended the smooth flame propagation regime up to 20 atm for H_2 and 30 atm for CH_4.

Figure 3 also shows that, for sufficiently off-stoichiometric CH_4 mixtures at high pressures, the low flame speed in conjunction with the increased density differential between the unburned and the burned gas enhance the buoyancy and thereby promote flame shape distortion. Fundamental flame speeds could not be extracted for these near-limit flames which are of great practical interest, e.g. in lean natural gas combustion for energy efficiency and pollution control.

REFERENCES

[1] Tse, S.D., Zhu, D.L., and Law, C.K. *A High-Pressure Combustion Apparatus* (2000), in preparation.
[2] Tse, S.D., Zhu, D.L. and Law, C.K. *Proc. Combust. Inst.* 28 (2000), in press.
[3] Rozenchan, G., Tse, S.D., Zhu, D.L. and Law, C.K. *AIAA* 2001-1080 (2001).
[4] Rozenchan, G. *M.S.E. Thesis*, Princeton University (2001), in preparation.
[5] Davis, S.G. and Law, C.K. *Combust. Sci. and Tech.* 140:427-449 (1998).
[6] Vagelopoulos, C.M., Egolfopoulos, F.N. and Law, C.K. *Proc Combust. Inst.* 25:1341 (1994).
[7] Taylor, S.C. *Ph.D. Thesis*, University of Leeds (1991).
[8] Sun, C.J., Sung, C.J., He, L. and Law, C.K. *Combust. Flame* 118:108-128 (1999).
[9] Law, C.K. and Sung, C.J. *Prog. Energy Combust. Sci.* 26:459-505 (2000).
[10] Kee, R.J., Grcar, J.F., Smooke, M.D. and Miller, J.A. SAND85-8240 (1985).
[11] Mueller, M.A., Kim, T.J., Yetter, R.A., Dryer, F.L. *Int. J. Chem. Kinet.* 31:113-125 (1999).
[12] Smith, G.P., Golden, D.M., Frenklach, M., Moriarty, N.W., Eiteneer, B., Goldenberg, M., Bowman, C.T., Hanson, R.K., Song, S., Gardiner Jr., W.C., Lissianski, V.V. and Qin, Z. *http://www.me.berkeley.edu/gri_mech/*
[13] Bechtold, J.K. and Matalon, M. *Combust. Flame* 67:77-90 (1987).
[14] Manton, J., Von Elbe, G. and Lewis, B. *J. Chem. Phys.* 20:153-157 (1952).